Dynamical freeze-out in three-fluid hydrodynamics

V. N. Russkikh[1,2,*] and Yu. B. Ivanov[1,2,†]
[1]*Gesellschaft für Schwerionenforschung mbH, Planckstr. 1, D-64291 Darmstadt, Germany*
[2]*Kurchatov Institute, Kurchatov sq. 1, RU-123182 Moscow, Russia*
(Received 29 November 2006; revised manuscript received 13 September 2007; published 14 November 2007)

The freeze-out procedure accepted in a model of three-fluid dynamics is analyzed. This procedure is formulated in terms of drain terms in hydrodynamic equations. The dynamics of freeze-out is illustrated by one-dimensional simulations. It is demonstrated that the resulting freeze-out reveals a nontrivial dynamics depending on initial conditions in the expanding "fireball." The freeze-out front is not just defined "geometrically" on the condition of the freeze-out criterion met but rather is a subject of fluid evolution. It competes with the fluid flow and does not always reach the place where the freeze-out criterion is met. Dynamics of the freeze-out in three-dimensional simulations is analyzed. It is demonstrated that the late stage of central nuclear collisions at the top energies available at the CERN Super Proton Synchrotron is of the form of three (two baryon-rich and one baryon-free) fireballs separated from each other.

DOI: 10.1103/PhysRevC.76.054907 PACS number(s): 24.10.Nz, 25.75.−q

I. INTRODUCTION

Hydrodynamics is now a conventional approach used to simulate heavy-ion collisions. Even review papers [1–5] do not comprise a complete list of the numerous applications of this approach. The hydrodynamics is applicable to describe the hot and dense stage of nuclear matter, when the mean free path is much shorter than the size of the system. However, as expansion proceeds, the system becomes dilute, the mean free path becomes comparable to the system size, and hence the hydrodynamic calculation should be stopped at some instant. All hydrodynamic calculations are terminated by a freeze-out procedure, while these freeze-out prescriptions are somewhat different in different models.

In the present paper, we would like to describe in more detail the freeze-out procedure accepted in a recently developed three-fluid dynamics (3FD) model [6,7]. The 3FD model is designed to simulate heavy-ion collisions in the energy range from the BNL Alternating Gradient Synchrotron (AGS) to the CERN Super Proton Synchrotron (SPS). Unlike conventional hydrodynamics, where local instantaneous stopping of projectile and target matter is assumed, a specific feature of the dynamic three-fluid description is a finite stopping power resulting in a counter-streaming regime of leading baryon-rich matter. The basic idea of a three-fluid approximation to heavy-ion collisions [6,7] is that at each space-time point a generally nonequilibrium distribution function of baryon-rich matter can be represented as a sum of two distinct locally equilibrated contributions, initially associated with constituent nucleons of the projectile (p) and target (t) nuclei. In addition, newly produced particles, populating the midrapidity region, are associated with a "fireball" (f) fluid. This model is a straightforward extension of the two-fluid model with radiation of direct pions [3,8,9] and the (2+1)-fluid model [10–12]. In particular, the 3FD model allows a certain formation time for the fireball-fluid production, during which the matter of the fluid propagates without interactions.

We have started our simulations [6,13,14] with a simple hadronic equation of state (EOS) [15]. This EOS is a natural reference point for any other more elaborate EOS. The 3FD model turned out to be able to reasonably reproduce a large body of experimental data [6,13,14] in a wide energy range from AGS to SPS. This was done with the unique set of model parameters summarized in Ref. [6]. Problems were met in describing transverse flow [13]. The directed flow required a softer EOS at top AGS and SPS energies (in particular, this desired softening may signal the occurrence of a transition into the quark-gluon phase).

In particular, transverse-mass spectra of various hadrons were reproduced [6,14]. Experimental data on transverse-mass spectra of kaons produced in central Au+Au [16] or Pb+Pb [17] collisions reveal peculiar dependence on the incident energy. The inverse-slope parameter (so-called effective temperature) of these spectra at midrapidity increases with incident energy in the AGS energy domain and then saturates at the SPS energies. In Refs. [18,19] it was assumed that this saturation is associated with the deconfinement phase transition. This assumption was indirectly confirmed by the fact that microscopic transport models, based on hadronic degrees of freedom, failed to reproduce the observed behavior of the kaon inverse slope [20]. Hydrodynamic simulations of Ref. [21] succeeded in describing this behavior provided the incident-energy dependence of the freeze-out temperature has a very similar shape to that of the corresponding kaon effective temperature. Thus, the puzzle of kaon effective temperatures was just translated into a puzzle of freeze-out temperatures.

In Ref. [14] it was shown that the dynamical description of freeze-out, accepted in the 3FD model, naturally explains the incident energy behavior of inverse-slope parameters of the transverse-mass spectra observed in experiments. This freeze-out dynamics, effectively resulting in a pattern similar to that of the dynamic liquid-gas transition, differs from conventionally used freeze-out schemes. This is the prime reason why we would like to return to discussion of assumptions underlying

*russ@ru.net
†Y.Ivanov@gsi.de

this prescription and present one-dimensional simulations, clarifying the consequences of this freeze-out. It is natural to start this discussion with a critical review of standard assumptions of the freeze-out and recent developments in this field.

II. FREEZE-OUT: A STILL DEBATED PROBLEM

Hydrodynamic simulation is terminated by a freeze-out procedure. Though this method (as applied to high-energy physics) was first proposed almost 50 years ago by Milekhin [22], this is a still debated problem. The method was intuitively clear and easily applicable. However, Cooper and Frye [23] claimed that Milekhin's method violates the law of energy conservation. To remedy the situation, they proposed their own recipe, in which the observable spectrum of a hadrons is calculated as

$$E\frac{dN_a}{d^3p} = \int_\Sigma d\sigma \left(p_\mu n_\sigma^\mu\right) f_a(p,x) \tag{1}$$

where Σ is a three-dimensional hypersurface on which a certain criterion of the freeze-out is met. Here integration runs over this hypersurface, n_σ^μ is normal vector to the element $d\sigma$ of this hypersurface, and $f_a(p,x)$ is an equilibrium distribution function of a hadrons, that is,

$$f_a(p,x) = \frac{g_a}{(2\pi)^3}\frac{1}{\exp\{(p_\mu u^\mu - \mu_a)/T\} \pm 1}, \tag{2}$$

defined in terms of local thermodynamic and hydrodynamic quantities on this freeze-out hypersurface: chemical potential $\mu_a(x)$, temperature $T(x)$, and four-velocity $u^\mu(x)$. Here g_a is degeneracy of the a particle.

The Cooper-Frye recipe [23] is now extensively used in hydrodynamic calculations, see, e.g., Refs. [24–36]. However, it is not free of problems either. It gives a negative contribution to the particle spectrum in some kinematic regions in which the normal vector to the freeze-out hypersurface is spacelike, $p_\mu n_\sigma^\mu < 0$. This negative contribution corresponds to frozen-out particles returning to the hydrodynamic phase. Cutoff of this negative contribution again returns us to the violation of energy conservation. To get rid of this negative spectrum, a modification of the Cooper-Frye recipe was proposed based on a cut-Jüttner distribution [37–40]. In this distribution, the part of the Jüttner distribution that gives the negative spectrum is simply cut off. To preserve the particle and energy conservation, the rest of the Jüttner distribution is renormalized, effectively resulting in a new temperature and chemical potential (so-called freeze-out shock). In fact, this cut-Jüttner recipe has no physical justification, except for practical utility. Moreover, the cut-Jüttner recipe is not supported by schematic kinetic treatment [41] of the transitional region from the hydrodynamic regime to that of dilute gas. Recently, there was proposed a new freeze-out recipe, a canceling-Jüttner distribution [42], which complies with the results of schematic kinetic treatment [41]. It should be stressed that this was precisely the schematic kinetic treatment. This region where the transition from highly collisional dynamics to the collisionless one occurs is highly difficult for the kinetic treatment and hardly allows any justified simplifications.

All the above considerations of the freeze-out process, including both the original Cooper-Frye prescription and its improvements, proceed from the following assumptions:

(i) "Decoupling" of matter from the hydrodynamic regime happens on *a continuous hypersurface* Σ.
(ii) This hypersurface is determined on the requirement that *a certain criterion of the freeze-out is met*: e.g., temperature, energy density, or baryon density reaches a certain value.
(iii) After this decoupling, particles *stream freely* to detectors.

In fact, transition from the highly collisional (hydro) regime to a collisionless one occurs in some finite four-volume. Assumption I is just an idealization—this four-volume is shrunk to a hypersurface. Conservation conditions on such a hypersurface are constructed in analogy with a shock front in hydrodynamics and result in the Cooper-Frye formula (1). However, the requirement that this surface is continuous does not follow from anywhere. It is just an assumption. For instance, if we assume a discontinuous hypersurface, i.e., that consisting of tiny (infinitely small in the continuum limit) fragments with normal vectors coinciding with the local four-velocity, $n_\sigma^\mu = u^\mu$, then we return to the original Milekhin's method of freeze-out.

Milekhin's method assumes that a hydrodynamic system freezes out by emitting tiny fireballs of matter. Let $P_{\rm tot}^\mu$ be the total four-momentum of the system. Then at the first step of the freeze-out, a tiny droplet with the four-momentum ΔP_i^μ is emitted,

$$P_{\rm tot}^\mu = P_{\rm fluid}^\mu + \Delta P_i^\mu, \tag{3}$$

where $P_{\rm fluid}^\mu$ is the four-momentum of the still hydro-evolving fluid. In terms of the energy-momentum tensor $T_{(i)}^{\mu\nu}$, the ΔP_i^μ four-momentum can be written as

$$\Delta P_i^\mu = \int_{\Delta V_i} dV\, T_{(i)}^{\mu 0} = \int_{\Delta\Sigma_i} d\sigma\, T_{(i)\nu}^{\mu} n_\sigma^\nu, \tag{4}$$

where ΔV_i is the volume of the fireball in the reference frame, where $T_{(i)}^{\mu 0}$ is considered. The last equality in Eq. (4) represents ΔP_i^μ in the covariant way, i.e., in terms of a hypersurface element $\Delta\Sigma_i$ and the normal vector to this element n_σ^μ, cf. Eq. (1). In particular, Milekhin's choice consists in $n_\sigma^\mu = u^\mu$. From representation (4) it may seem that the relation between ΔP_i^μ and $T_{(i)}^{\mu\nu}$ depends on $\Delta\Sigma_i$. This would imply that a proper hypersurface element $\Delta\Sigma_i$ should be chosen to maintain relation (4). In fact, the right-hand side of Eq. (4) is independent of n_σ^μ. The formal proof of that can be found, e.g., in Ref. [43]. It is possible to demonstrate it in a simpler way. Let us write down $T_{(i)}^{\mu 0}$ in terms of contributions of individual particles [43]

$$T_{(i)}^{\mu 0}(\mathbf{x},t) = \sum_n p_n^\mu(t)\delta^3(\mathbf{x} - \mathbf{x}_n(t)), \tag{5}$$

where $p_n^\mu(t)$ and $\mathbf{x}_n$ are the four-momentum and the instant position of the nth particle, respectively. Integrating expression

(5) over volume ΔV_i, according to Eq. (4), we arrive at

$$P_i^\mu = \sum_n p_n^\mu(t). \tag{6}$$

Here, spurious dependence on $\Delta\Sigma_i$ reveals itself in a seeming dependence of the right-hand side of Eq. (6) on the synchronized time instant t, which really depends on the reference frame and hence on $\Delta\Sigma_i$. Note that the P_i^μ quantity is assumed to be conserved; therefore, the time dependence of the right-hand side of Eq. (6) is completely inappropriate.

Let us consider the right-hand side of Eq. (6) in two reference frames, i.e., on two hypersurface elements $\Delta\Sigma_i$ and $\Delta\Sigma_i'$. The time synchronization depends on the reference frame. Therefore, in the sums over particles

$$\sum_n p_n^\mu(t) \quad \text{and} \quad \sum_n p_n'^\mu(t') \tag{7}$$

some $p_n^\mu(t)$ and $p_n'^\mu(t')$ may occur which are not simply related by the Lorentz transformation but are completely different, because the corresponding particles at the t' instant have exercised additional interactions (or, vice versa, have not exercised all those interactions) as compared to those completed to the t instant. And nevertheless two sums in Eq. (7) are equal, since in each two-particle or multiparticle *pointlike* interaction the four-momentum is conserved. The pointlike character[1] of the interaction is of prime importance here. If particles interact pointlike, they change their momenta simultaneously in any reference frame. Thus, the right-hand side of Eq. (6) is really independent of time t and hence of $\Delta\Sigma_i$.

In view of Eqs. (3) and (4), upon completion of the freeze-out process, we have

$$P_{\text{tot}}^\mu = \sum_i \Delta P_i^\mu = \sum_i \int_{\Delta\Sigma_i} d\sigma T_{(i)\nu}^\mu n_\sigma^\nu = \int_\Sigma d\sigma T_\nu^\mu n_\sigma^\nu, \tag{8}$$

where the hypersurface Σ consists of elements $\Delta\Sigma_i$. As we have seen, this four-momentum conservation does not depend on the choice of hypersurface elements $\Delta\Sigma_i$. Milekhin's choice is $n_\sigma^\mu = u^\mu$ and results in a discontinuous hypersurface. The Cooper-Frye choice proceeds from the requirement of continuity of the Σ hypersurface. The difference between these two choices is illustrated in Fig. 1. The lower panel of Fig. 1 shows a schematic structure of Milekhin's hypersurface. In practical calculations, the fragments of Milekhin's hypersurface are so tiny that the whole hypersurface looks like that in the upper panel of Fig. 1, however, with the normal vector to each tiny fragment coinciding with the four-velocity.

Therefore, Milekhin's method in fact conserves energy, but to see it one should consider it on a discontinuous hypersurface. The baryon number conservation can be demonstrated in a similar way. The fact that different single-particle distributions (i.e., Cooper-Frye, cut-Jüttner with renormalization, canceling-Jüttner, and even Milekhin's distributions) provide

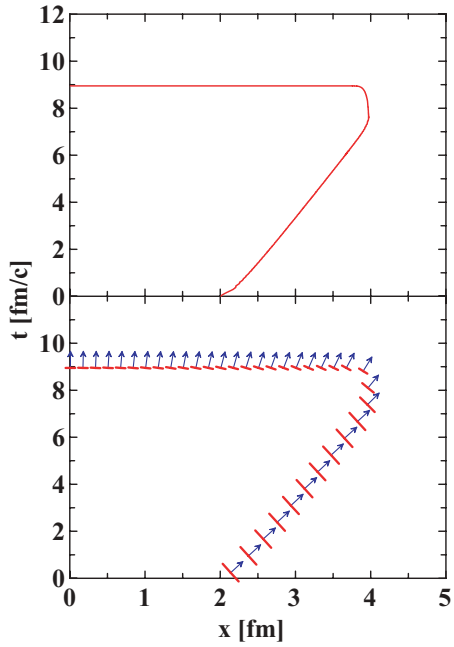

FIG. 1. (Color online) Freeze-out hypersurface for hydrodynamic evolution of the one-dimensional (1D) steplike slab of nuclear matter (see Sec. III C). Initial conditions for this slab are constructed on the assumption that they are formed by the shock-wave mechanism in head-on collisions of two 1D slabs at $E_{\text{lab}} = 10A$ GeV. The upper panel displays the Cooper-Frye choice for the hypersurface. The lower panel schematically illustrates Milekhin's choice for the hypersurface. Arrows indicate local four-velocities on this hypersurface.

all the required conservation laws and at the same time produce different particle spectra, cf. Eq. (1) and Refs. [23,44], only increases the ambiguity of freeze-out consequences and indicates the barest necessity for further studies of freeze-out. Such studies of freeze-out in a finite four-volume (a finite spacelike layer [45]) are now in progress.

From a practical point of view, assumption II means that we should first run the hydrodynamic calculation without any freeze-out and only after that look for a hypersurface, where the freeze-out criterion is met. This hypersurface is determined as if the hydrodynamic system is not affected by the freeze-out. This procedure indeed results in a continuous hypersurface, which could justify assumption I. The method of "continuous emission" [46] offers a more consistent way of performing freeze-out. This method considers a continuous emission of particles from a finite volume, governed by their mean free paths. In this approach, the freeze-out process looks like an evaporation (or fragmentation, on account of the final-size grid) first from the system surface and then as a volume fragmentation of the system residue. The particle emission from the surface layer of the mean-free-path width may hint at a discreetness of the hypersurface arising when this width is shrunk to zero.

In particular, the continuous-emission mechanism implies that dynamics of this evaporation, characterized by its own rate, competes with the hydrodynamic expansion. Therefore, the freeze-out front may not reach the places where, e.g., the

[1]Action at distance in the relativistic case requires introduction of fields mediating this interaction. Then the field contribution should be also included in $T^{\mu 0}$. For the sake of simplicity, we confine ourselves to the pointlike interaction.

energy density reaches the critical value. This is already a consequence of real freeze-out dynamics. Unfortunately, this method is very difficult for the numerical implementation because the probability of a particle leaving the hydrodynamic system depends not only on the past but also on the future evolution of this system, since particle emission occurs from a time-evolving system.

Assumption III is also an approximation to reality. This was the reason why cascading was applied after the hydrodynamic freeze-out in Refs. [26,29,34,35]. This cascading allowed one, in particular, to reproduce a two-slope form of transverse-mass spectra [26] and a correct value of elliptic flow [27,28]. Inclusion of some inelastic channels in this cascading may be important for the proper reproduction of multiplicities, e.g., the K^- multiplicity [6]. However, even this cascading is not enough. A mean-field cascading is really needed. The reasons for this are as follows. First of all, matter at the freeze-out instant is still dense enough, such that a part of the energy is accumulated in collective mean fields. This mean-field energy should be released before calculating observables. In the presently discussed 3FD model [6], we do this at the freeze-out stage by recalculating thermodynamic quantities in terms of the hadronic gas EOS rather than a nontrivial EOS used in the hydrodynamic computation.

III. FREEZE-OUT IN 3FD

The freeze-out scheme adopted in the 3FD model is an attempt to modify and improve the standard freeze-out procedure in certain aspects rather than a final solution of the freeze-out problem. Let us start with the criteria of the freeze-out. We formulate these criteria in terms of energy density, which is a universal quantity applicable both at very high energies (instead of temperature) and at low energies (instead of baryon density).

(i) The freeze-out criterion we use is

$$\varepsilon < \varepsilon_{\rm frz}, \tag{9}$$

where

$$\varepsilon = u_\mu T^{\mu\nu} u_\nu \tag{10}$$

is the total energy density of all three fluids in the proper reference frame, in which the composed matter is at rest. This total energy density is defined in terms of the total energy-momentum tensor

$$T^{\mu\nu} \equiv T_{\rm p}^{\mu\nu} + T_{\rm t}^{\mu\nu} + T_{\rm f}^{\mu\nu} \tag{11}$$

being the sum over the energy-momentum tensors of separate fluids, and the total collective four-velocity of the matter

$$u^\mu = u_\nu T^{\mu\nu}/(u_\lambda T^{\lambda\nu} u_\nu). \tag{12}$$

Note that definition (12) is, in fact, an equation determining u^μ. In general, this u^μ does not coincide with four-velocities of separate fluids. This definition of the collective four-velocity is in the spirit of the Landau-Lifshitz approach to viscous relativistic hydrodynamics [47]. Only the formed (to the time instant of consideration) part of the f-fluid is taken into account in $T_{\rm f}^{\mu\nu}$ of Eq. (11). To the end of the freeze-out process all f-fluid turns out to be formed and hence frozen out. In the present simulations, we use the value $\varepsilon_{\rm frz} = 0.4$ GeV/fm^3 as the critical freeze-out energy density, with the exception of low incident energies $E_{\rm lab}$, for which we use lower values: $\varepsilon_{\rm frz}(2A\ \text{GeV}) = 0.3$ GeV/fm^3 and $\varepsilon_{\rm frz}(1A\ \text{GeV}) = 0.2$ GeV/fm^3.

(ii) To prevent freeze-out of the initial cold nuclei, we apply the additional criterion

$$u_\mu \partial^\mu \varepsilon < 0 \quad \text{at the system surface,} \tag{13}$$

i.e., at the border of matter with vacuum, which coincides with the freeze-out front. In the frame where the freeze-out front is at rest, $\partial_t \varepsilon = 0$, condition (13) reduces to $\mathbf{u}\nabla\varepsilon < 0$, which demands that the collective velocity of matter is directed outside the system. To meet this condition, we in fact start the freeze-out procedure only at the expansion stage of the collision (see next section).

(iii) A very important feature of our freeze-out procedure is an antibubble prescription, preventing the formation of bubbles of frozen-out matter inside the dense matter still hydrodynamically evolving. The matter is allowed to be frozen out (provided the two above criteria are met) only if either (a) the matter is located near the boarder with vacuum (this piece of matter gets locally frozen out) or (b) the maximal value of the total energy density in the system is less than $\varepsilon_{\rm frz}$

$$\max \varepsilon \leqslant \varepsilon_{\rm frz} \tag{14}$$

(the whole system gets instantly frozen out).

Criterion (iii b) is convenient for numerical implementation, while it does not look quite physical. From a physical point of view, it would be preferable to change $\max \varepsilon$ to the energy density averaged over the system, $\langle\varepsilon\rangle$. In view of the discussion below, such a substitution would not change the qualitative pattern of the freeze-out; however, it could somewhat affect quantitative results at AGS energies.

Before the instant of the global freeze-out, cf. (iii b), the above freeze-out criteria can be summarized in terms of the dynamic equations

$$\partial_\mu J_\alpha^\mu = \Theta_{\rm frz} J_\alpha^\mu \partial_\mu \Theta_{\rm s}, \tag{15}$$

$$\partial_\mu T_\alpha^{\mu\nu} = (\text{Friction})^\nu + \Theta_{\rm frz} T_\alpha^{\mu\nu} \partial_\mu \Theta_{\rm s}, \tag{16}$$

where J_α^μ is the baryon current of the α fluid, $\alpha =$ p, t or f (i.e., projectile, target, or fireball); note that $J_{\rm f}^\mu \equiv 0$. Here $(\text{Friction})^\nu$ stands for interaction terms between fluids, the explicit form of which is not important here. $\Theta_{\rm s}$ is a step function at the system surface, which takes into account criterion (iii a). One-dimensional simulations of the freeze-out (i)–(iii a) show that it results in discontinuity of ε (and other quantities) at the system surface. This discontinuity is numerically smeared out only to the extent of the finite grid step. Therefore, in analytic equations, the step function $\Theta_{\rm s}$ can be represented by a sharp step function

$$\Theta_{\rm s} = \Theta(\varepsilon - \delta), \tag{17}$$

with $\delta \to +0$. The function

$$\Theta_{\rm frz} = \Theta(\varepsilon_{\rm frz} - \varepsilon^s)\Theta(-u_\mu \partial^\mu \varepsilon), \tag{18}$$

with ε^s being the value of ε at the matter side of the surface discontinuity, takes into account conditions (i) and (ii) of the freeze-out. Let freeze-out conditions (i) and (ii) be met, i.e., $\Theta_{\rm frz} = 1$. To verify that Eqs. (15)–(18) actually correspond to the above-described scheme (i)–(iii a), let us consider these equations for the stationary situation in the reference frame, where the freeze-out front is at rest, i.e., $\partial_t \Theta_{\rm s} = 0$. For the sake of convenience, let us associate the freeze-out front with the $x = 0$ plane. Then the only nonzero component of the $\partial_\mu \Theta_{\rm s}$ four-vector is $\partial_x \Theta_{\rm s} = -\delta(x)$ (the hydrodynamic matter occupies the $x < 0$ semi-space), and Eqs. (15) and (16) take the form

$$\partial_x J^x_\alpha = -J^x_{\alpha(s)}\delta(x),$$
$$\partial_x T^{xy}_\alpha = -T^{xy}_{\alpha(s)}\delta(x),$$

where symbol (s) in the subscript indicates that the value is taken at the matter side of the freeze-out front. The latter is the effect of $\delta \to +0$ introduced in Eq. (18). We have also omitted friction forces in the right-hand side of Eq. (16), since they are really unimportant at the freeze-out stage. Integrating the above equations over small Δx around $x = 0$, we arrive at

$$\Delta J^x_\alpha \equiv J^x_{\alpha(x>0)} - J^x_{\alpha(s)} = -J^x_{\alpha(s)},$$
$$\Delta T^{xy}_\alpha \equiv T^{xy}_{\alpha(x>0)} - T^{xy}_{\alpha(s)} = -T^{xy}_{\alpha(s)}.$$

Thus, terms $\propto \partial_\mu \Theta_{\rm s}$ in the right-hand side of Eqs. (15) and (16) play the role of sinks, which remove matter from hydrodynamic evolution, making the hydrodynamic quantities $J_{\alpha(x>0)}$ and $T_{\alpha(x>0)}$ to be zero after the freeze-out front.

This kind of freeze-out is similar to the model of continuous emission proposed in Ref. [46]. There the particle emission occurs from a surface layer of the mean-free-path width. In our case, the physical pattern is similar, only the mean free path is shrunk to zero.

The above discussion concerns only the first part of the freeze-out procedure, i.e., the application of freeze-out conditions. The second part consists in the calculation of the spectra of observable particles:

(iv) Milekhin's method [22], defined on a discontinuous hypersurface, was used for calculation of observables, cf. Sec. II.

Thus, this freeze-out is similar to the evaporation of particles from a free surface of the system followed by explosion of the fluid residue, if criterion (9) is met in the whole finite volume of this residue.

A. Physical pattern of the freeze-out

The physical pattern behind this freeze-out resembles the process of expansion of a compressed and heated classical fluid into a vacuum. The physics of this process has been studied both experimentally and theoretically [48–51]. Evaporation from the free surface of a normal (not superheated) fluid is a very slow process. Accordingly, the freeze-out of matter of high density ($\varepsilon > \varepsilon_{\rm frz}$) is suppressed in our model. During expansion, the fluid becomes more rarefied, still remaining quite hot. Thus, the fluid becomes superheated at $\varepsilon < \varepsilon_{\rm frz}$. It occurs first at the periphery of the system, which is first affected by the decompression wave. Evaporation from the free surface of a superheated fluid is already a fast process. Accordingly, the freeze-out is allowed at $\varepsilon < \varepsilon_{\rm frz}$.

Situations are possible in which the freeze-out criterion (9) is met in the whole slab near the free surface rather than only at the surface. Such situations are illustrated in Secs. III C and III D. Here we have a choice to either instantaneously freeze-out this whole near-surface slab or wait until the freeze-out front will gradually traverse this slab (if ever). Making this choice, we rely on the results of experiments on evaporation from superheated fluids. It was shown (see, e.g., Ref. [51]) that the evaporation front propagates with respect to the fluid not faster than with the speed of sound. Precisely this choice is realized in our model by means of condition (iii a) or alternatively by dynamic equations (15) and (16). Thus, the freeze out front may stay at essentially lower energy densities than $\varepsilon_{\rm frz}$, because supersonic fluid expansion prevents it from reaching the region, where $\varepsilon = \varepsilon_{\rm frz}$.

Physically it implies that a particle is evaporated (frozen out) only if it escapes from the system without collisions. Thus, its mean free path ($\lambda_{\rm mfp}$) should be larger than its path to the free surface (with due account of the future evolution of the fluid). Precisely this criterion is applied in the model of continuous emission [46]. In our simplified version of the continuous emission, $\lambda_{\rm mfp} = 0$ in the fluid phase and $\lambda_{\rm mfp} \to \infty$ in the gas phase. Therefore, a particle can escape only from the free surface, which cannot move into the system faster than with the speed of sound [51]. The only exception to this rule occurs at the final stage of the freeze-out. As it was observed in experiments with classical fluids (see, e.g., Ref. [49]), a fluid transforms into gas by explosion if it is strongly superheated all over its volume. Therefore, at the final stage of the freeze-out, when criterion (9) is met in the whole volume of the fluid residue, we assume that the whole residue becomes frozen out simultaneously [condition (iii b)].

Of course, criterion (9) is not universal. In particular, it is not applicable to cold nuclear matter, which has $\varepsilon \approx 0.15\,{\rm GeV/fm}^3$ in its ground state. Additional condition (13), preserving the cold nuclear matter from being frozen out, is directly connected with this fact. We hope that criterion (9) is good enough for a restricted domain of the phase diagram, where freeze-out of hot nuclear matter really occurs.

To further clarify our freeze-out scheme, it is useful to consider the way it was implemented in the numerical scheme.

B. Numerical implementation of freeze-out

The numeric scheme of the 3FD code is based on the modified particle-in-cell method [52,53], which is an extension of the scheme first applied at LANL [54]. In the particle-in-cell method, each time step of the computation consists of three stages: (I) Eulerian stage, (II) Lagrangian stage, and (III)

transformation from the frame of computation to the local rest frame of fluids in order to calculate thermodynamic quantities and flow velocities [as applied to the freeze-out, it is described in point (c) of this section].

The transfer of energy-momentum due to pressure gradients, friction between fluids, and production of the fireball fluid is computed on the spatially fixed grid (so-called Eulerian stage of the scheme). The convective transfer of the baryonic charge, energy, and momentum is performed at the Lagrangian stage of the scheme. At this stage, the matter is represented by an ensemble of Lagrangian particles which accumulate all the energy, momentum, and baryon charge of the system. At the time step (let it be "1") when the freeze-out has not started yet, the total energy-momentum $P^{\mu}_{\rm tot}$ and baryon charge $B_{\rm tot}$ are presented by sums over these particles, that is,

$$P^{\mu}_{\rm tot} = \sum_{i\alpha} \Delta P^{\mu}_{i\alpha}(t_1) = \sum_{i\alpha} \Delta V_{i\alpha}(t_1)\, T^{\mu 0}_{(i\alpha)}(t_1), \qquad (19)$$

$$B_{\rm tot} = \sum_{i\alpha} \Delta B_{i\alpha}(t_1) = \sum_{i\alpha} \Delta V_{i\alpha}(t_1)\, J^{0}_{(i\alpha)}(t_1), \qquad (20)$$

where $\Delta P^{\mu}_{i\alpha}(t_1)$ and $\Delta B_{i\alpha}(t_1)$ are, respectively, the energy-momentum and baryon charge of an ith particle belonging to the α fluid. These sums run over both formed and still unformed particles of the f fluid. In fact, baryon charges of all particles belonging to a baryon-rich fluid are taken to be constant and equal, $\Delta B_{ip}(t) = b_p$ and $\Delta B_{it}(t) = b_t$ ($b_p = b_t$ if nuclei are identical); while for the f-fluid, $\Delta B_{if}(t) = 0$. Each Lagrangian particle is also characterized by a volume $\Delta V_{i\alpha}(t_1)$. Therefore, the above quantities of the particle are expressed in terms of respective densities $T^{\mu 0}_{(i\alpha)}$ and $J^{0}_{(i\alpha)}$, as indicated in Eqs. (19) and (20). Simulation is performed in the frame of equal velocities of colliding nuclei. Hence, all the quantities in Eqs. (19) and (20) are related to this frame. Equations (19) and (20) imply that all the matter participates in dynamical evolution before the freeze-out starts:

$$P^{\mu}_{\rm dyn}(t_1) = P^{\mu}_{\rm tot}, \quad B_{\rm dyn}(t_1) = B_{\rm tot}. \qquad (21)$$

Here $P^{\mu}_{\rm dyn}$ and $B_{\rm dyn}$ are, respectively, total energy-momentum and baryon charge participating in dynamical evolution. We avoid the term "hydrodynamic evolution" because a part of the f fluid may be still unformed.

In the present scheme, the Lagrangian particle has a profile function of the form and size of the grid cell with uniform distribution of densities. Therefore, in three-dimensional (3D) simulations, a single Lagrangian particle contributes to eight cells on the grid, with which it overlaps. These spatially extended particles make the scheme smoother and hence more stable. In Refs. [3,6] this numerical scheme is described in more detail. Within this scheme the freeze-out proceeds as follows:

(a) To roughly meet condition (ii), the freeze-out procedure is started only at the expansion stage of the collision, i.e., after the time interval required for nuclei to traverse each other, provided they keep their initial velocities. In the c.m. frame of two identical nuclei this time delay is $\Delta t_{\rm frz} = D_A/(\gamma_{\rm c.m.} v_{\rm c.m.})$, where $D_A/\gamma_{\rm c.m.}$ is the Lorentz contracted diameter of the nucleus, $\gamma_{\rm c.m.}$ and $v_{\rm c.m.}$ are the γ factor and the initial velocity of the nucleus in the c.m. frame, respectively.

(b) The freeze-out criterion (9) is checked at the Lagrangian stage of each time step (let it be the nth step). In the f fluid, only those particles are considered which have been formed to the time instant t_n. For each Lagrangian particle, it is checked in all cells, which overlap with this considered particle, i.e., in eight cells. If the freeze-out criterion is met in *all these eight cells* and if at least one of these cells is "empty" (i.e., contains no centers of any Lagrangian particles), then this considered Lagrangian particle is counted as frozen out. This is the realization of condition (iii a). This frozen-out Lagrangian particle is removed from further hydrodynamic evolution. By doing this, we remove respective portions from sums (19) and (20):

$$P^{\mu}_{\rm dyn}(t_n) = P^{\mu}_{\rm dyn}(t_{n-1}) - \sum_{i\alpha \text{ frozen out at } t_n} \Delta P^{\mu}_{i\alpha}(t_n), \qquad (22)$$

$$B_{\rm dyn}(t_n) = B_{\rm dyn}(t_{n-1}) - \sum_{i\alpha \text{ frozen out at } t_n} \Delta B_{i\alpha}(t_n). \qquad (23)$$

Only parts $P^{\mu}_{\rm dyn}(t_n)$ and $B_{\rm dyn}(t_n)$ are kept in further dynamic evolution, unlike the conventional Cooper-Frye method. It is important to mention that had we kept this frozen-out particle in the dynamic evolution, its energy-momentum content would be changed at later time steps, and hence a part of its energy-momentum would be gained by other particles. Then we would face problems with the energy-momentum conservation, if we wanted to use the $\Delta P^{\mu}_{i\alpha}$ quantity at the instant of its freeze-out for the calculation of observable spectra.

If the freeze-out criterion is met in *all cells of the system*, all Lagrangian particles are counted as frozen out at this time step, as required by condition (iii b). This is the end of the freeze-out process.

(c) When the freeze-out process is over, i.e., $P^{\mu}_{\rm dyn} = 0$ and $B_{\rm dyn} = 0$, we are left with an ensemble of frozen-out Lagrangian particles which precisely obeys the conservation laws:

$$P^{\mu}_{\rm tot} = \sum_{i\alpha} \Delta P^{\mu}_{i\alpha}(t_{i\alpha\,\text{frozen-out}}), \qquad (24)$$

$$B_{\rm tot} = \sum_{i\alpha} \Delta B_{i\alpha}(t_{i\alpha\,\text{frozen-out}}). \qquad (25)$$

Here the summation runs over frozen-out (at different time instants $t_{i\alpha\text{frozen-out}}$) particles, unlike sums (19) and (20), where this summation is associated with a fixed time instant. These frozen-out particles are precisely those droplets mentioned in Eq. (3).

A frozen-out $i\alpha$ particle is still characterized by five hydrodynamic quantities, $J^{0}_{i\alpha}$ and $T^{\mu 0}_{i\alpha}$, and volume $\Delta V_{i\alpha}$, all these in the reference frame of computation. For the calculation of spectra, we need a distribution function formulated in terms of thermodynamic quantities: temperature ($T^{i\alpha}$), baryon ($\mu^{i\alpha}_{b}$) and strange ($\mu^{i\alpha}_{s}$) chemical potentials, and hydrodynamic four-velocity ($u^{\mu}_{i\alpha}$), cf. Eqs. (1) and (2). In fact, this recalculation of the hydrodynamic quantities into thermodynamic

ones is performed at each time step of the scheme based on the nongas EOS (involving some mean fields) accepted in the calculation. This EOS is not suitable for calculation of the spectrum of observable particles. First we should release the energy stored in mean fields. To do this, we calculate $T^{i\alpha(\mathrm{gas})}$, $\mu_b^{i\alpha(\mathrm{gas})}$, $\mu_s^{i\alpha(\mathrm{gas})}$, and $u^{\mu}_{i\alpha(\mathrm{gas})}$ based on *the hadronic gas EOS* and proceeding from conservations of total energy-momentum and baryon and strange charges in the frozen-out particle.

(d) At this stage, we are still free to choose either Cooper-Frye or Milekhin's scheme to calculate observables, as it was argued in Eqs. (3)–(8). We use Milekhin's method [22], defined on a discontinuous hypersurface consisting of tiny fragments coinciding with volumes of frozen-out Lagrangian particles $\Delta V_{i\alpha}$. The observable spectrum of hadrons is calculated as

$$E\frac{dN}{d^3p} = \sum_{i\alpha} V_{i\alpha}^{(\mathrm{proper})} p_\mu u^{\mu}_{i\alpha(\mathrm{gas})} f_{i\alpha(\mathrm{gas})}(p), \qquad (26)$$

where $V_{i\alpha}^{(\mathrm{proper})}$ is the volume of the $i\alpha$ particle in its rest frame, the sum runs over all frozen-out particles of all fluids, and $f_{i\alpha(\mathrm{gas})}(p)$ is the equilibrium distribution function defined already in terms of local *gas* thermodynamic ($T^{i\alpha(\mathrm{gas})}$, $\mu_b^{i\alpha(\mathrm{gas})}$, and $\mu_s^{i\alpha(\mathrm{gas})}$) and hydrodynamic ($u^{\mu}_{i\alpha(\mathrm{gas})}$) quantities, cf. Eqs. (1) and (2).

In this prescription, the baryon number and energy-momentum are precisely conserved by construction. It is worthwhile to mention that both the Cooper-Frye and Milekhin methods possess the same main problem: they do not reject contributions of frozen-out hadrons returning into the hydrodynamic phase and do this to precisely the same extent, see the Appendix. In particular, in our calculation, this problem probably reveals itself in the failure to reproduce the pion directed flow [6,13]. The advantage of Milekhin's method is just practical: with the exception of the pion directed flow, it quite successfully works in the 3FD model. The canceling-Jüttner recipe [42] overcomes the returning-hadrons problem of the above methods. It would be of interest to apply it in the 3FD model.

C. One-dimensional simulations

To clarify the physics described by Eqs. (15)–(18), let us consider one-dimensional (1D) simulations based on them. In Fig. 2, decays of steplike slabs of nuclear matter are presented. These simulations have been performed till the time instant of the global freeze-out, i.e., when criterion (iii b) is met. The same EOS as that used in three-dimensional (3D) simulations [6,13,14] is accepted in the present calculations. First of all, we see that the freeze-out front is really steplike. It is smeared only over two cells (independently of their size) due to the numeric scheme. Note also that for this steplike initial geometry, the supersonic flow of matter ($v_x > c_s$, where c_s is the speed of sound) always occurs beyond the initial boundary of the slab, while the flow within the initial boundary is always subsonic ($v_x < c_s$). This is important for understanding the results displayed in Fig. 2.

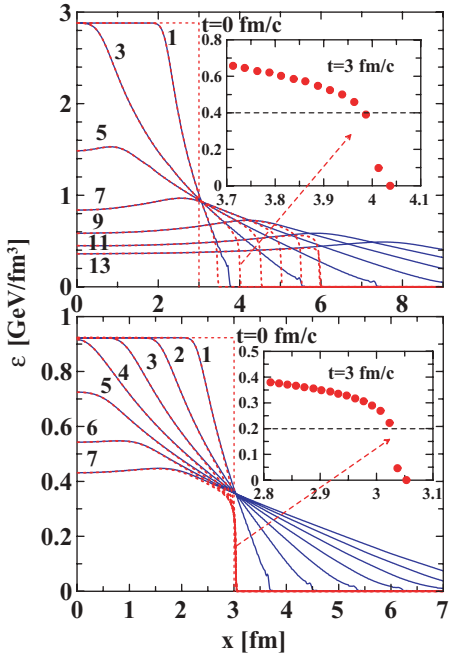

FIG. 2. (Color online) Evolution of the energy density during the decay of the 1D steplike slab of nuclear matter. Solid lines display calculations without freeze-out; dashed lines, with freeze-out. Initial conditions for these slabs are constructed on the assumption that they are formed by the shock-wave mechanism in the head-on collisions of two 1D slabs at $E_{\mathrm{lab}} = 10A$ GeV (upper panel) and $E_{\mathrm{lab}} = 2A$ GeV (lower panel). Insets show zoomed regions of the freeze-out front at the fixed time instant $t = 3$ fm/c in terms of the energy density in separate cells (displayed as dots).

There are three important velocities in this problem: the hydrodynamic velocity of the matter v_x at the position where the freeze-out front occurs, the speed of sound c_s, and the velocity v_ε of transfer of the constant value of $\varepsilon = 0.4$ GeV/fm^3:

$$\varepsilon(v_\varepsilon t + \mathrm{const}, t) = 0.4\ \mathrm{GeV/fm^3}. \qquad (27)$$

In fact, Eq. (27) is the equation for the hydrodynamic characteristic curve related to the 0.4 GeV/fm^3 value of the energy density. The freeze-out front, as defined by Eqs. (15) and (16), cannot propagate in the fluid medium faster than with the local speed of sound, like any perturbation in the hydrodynamics.

Different dynamic patterns of the freeze-out fronts displayed in the two panels of Fig. 2 are associated with different relations between the above three velocities. In the upper case of $\varepsilon_0 \simeq 3$ GeV/fm^3, we have $v_\varepsilon > 0$. Hence, the point where the freeze-out criterion (18) starts to be met is transferred farther and farther from the initial system boundary, and the system expands. In this region, the flow is supersonic: $v_x > c_s$. At the same time, the matter velocity with respect to the characteristic velocity is[2] $(v_x - v_\varepsilon)/(1 - v_x v_\varepsilon) \leqslant c_s$, i.e., it is less than the speed of sound. Therefore, the fluid flow does not carry the freeze-out front away from the point of

[2]Note that velocities are added relativistically.

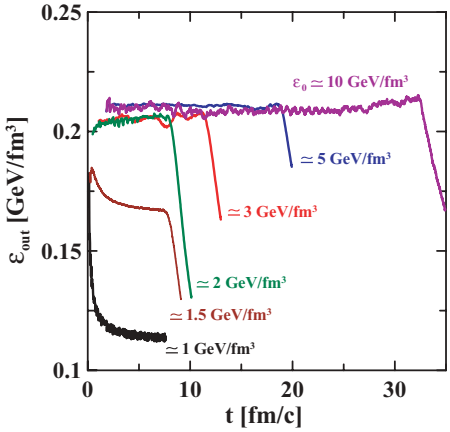

FIG. 3. (Color online) Instant values of actual energy density of the frozen-out matter for decays of nuclear-matter slabs with various initial conditions (labeled by initial energy densities ε_0). Initial conditions are constructed on the assumption of the shock-wave mechanism in head-on collisions of two slabs at $E_{\rm lab} = 2A, 4A, 6A, 10A, 20A$, and $40A$ GeV (from bottom left to top right). The time evolution is displayed up to the time instant of the global freeze-out (iii b).

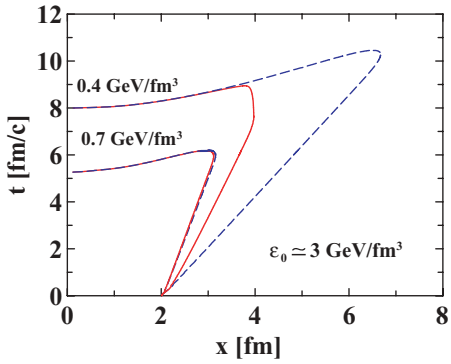

FIG. 4. (Color online) Characteristic curves for hydrodynamic evolution of the 1D steplike slab with initial conditions corresponding to the upper panel of Fig. 2. Solid lines display characteristic curves corresponding to $\varepsilon = 0.4$ and 0.7 GeV/fm^3, calculated with local freeze-out (iii a) but without global freeze-out (iii b). Dashed lines correspond to the calculation without freeze-out.

$\varepsilon = 0.4$ GeV/fm^3, where the freeze-out criterion (18) is met. The freeze-out front stays at this position, see the zoomed inset in the top panel of Fig. 2. Since the matter within this freeze-out front is distributed over the range of $0 < \varepsilon < 0.4$ GeV/fm^3, an average value for the actual energy density of the frozen-out matter (let us denote it as $\varepsilon_{\rm out}$) is approximately half of the freeze-out jump, i.e., $\varepsilon_{\rm out} \approx \varepsilon_{\rm frz}/2 = 0.2$ GeV/fm^3 in this case, see Fig. 3.

In the bottom panel of Fig. 2, i.e., $\varepsilon_0 \simeq 1$ GeV/fm^3, we have $v_\varepsilon < 0$. Here, the point where freeze-out criterion (18) starts to be met cannot be reached by the freeze-out front. Indeed, the freeze-out front is first formed beyond the initial boundary of the slab, i.e., in the region of the supersonic flow of the matter. Since it cannot be faster than sound, it cannot overcome the "supersonic barrier" in the back direction in order to reach the $\varepsilon = 0.4$ GeV/fm^3 point. It stays at the position of the supersonic barrier and does not move. Therefore, the decaying and freezing-out system does not expand. Moreover, the front stays at the position of low energy density, $\varepsilon \simeq 0.2$ GeV/fm^3, see the zoomed inset in the bottom panel of Fig. 2. Therefore, the actual energy density of the frozen-out matter turns out to be lower than $\varepsilon_{\rm frz}/2$ (as in the above case), i.e., $\varepsilon_{\rm out} \approx (0.2$ GeV/fm$^3/2 = 0.1$ GeV/fm^3, see Fig. 3.

In Fig. 3, we see that $\varepsilon_{\rm out}$ remains practically constant during the major period of the freeze-out. The steep fall of $\varepsilon_{\rm out}$ just before the global freeze-out occurs because the velocity v_ε on the characteristic curve (27) changes its sign. Then the point where $\varepsilon = 0.4$ GeV/fm^3 is achieved starts to rapidly move into interior of the system, and hence the freeze-out front remains at a lower energy density.

Thus, we see that the freeze-out is not inseparably linked with the freeze-out energy density $\varepsilon_{\rm frz}$ but can occur at lower energy densities for dynamical reasons. At low initial energy densities, the freeze-out front stays at lower energy densities than $\varepsilon_{\rm frz}$; hence the actual energy density of the frozen-out matter $\varepsilon_{\rm out}$ turns out to be lower than $\varepsilon_{\rm frz}/2$, see Fig. 3. With the initial energy density rising, the $\varepsilon_{\rm out}$ quantity grows and gradually reaches the $\varepsilon_{\rm frz}/2$ value and than approximately saturates.

A standard procedure for performing freeze-out, which is now applied in the major part of hydrodynamic calculations, proceeds in the following way. The hydrodynamic calculation runs absolutely unrestricted. The freeze-out hypersurface is determined by analyzing the resulting four-dimensional field of hydrodynamic quantities on the condition of the freeze-out criterion being met. In our case, this would be the characteristic curve of $\varepsilon = 0.4$ GeV/fm^3 calculated without freeze-out, displayed in Fig. 4.

In the 3FD model, the freeze-out criterion is checked continuously during the simulation. If some parts of the hydrodynamic system meet all criteria [(i), (ii), and either (iii a) or (iii b)], they decouple from the hydrodynamic calculation. The frozen-out matter escapes from the system, removing all the energy and momentum accumulated in it, cf. Eq. (3). Therefore, it produces no recoil to the rest of the still hydrodynamic system. The removal of the matter affects the system evolution. This influence is illustrated in Fig. 4. The $\varepsilon = 0.4$ GeV/fm^3 characteristic curves calculated with and without freeze-out turn out to be different. At the same time, the $\varepsilon = 0.7$ GeV/fm^3 characteristic curves, which lie quite deep inside the system, remain unaffected by the freeze-out. The freeze-out hypersurface (i.e., the curve in 1+1 dimensions) for this case is presented in Fig. 1. It differs from the corresponding characteristic curve because of the global freeze-out which occurs at time instant $t \simeq 9$ fm/c.

It is of interest to compare particle spectra predicted by different models for freeze-out. In Fig. 5, rapidity distributions of various hadrons are demonstrated for three different prescriptions of the freeze-out: the above-described model of dynamical freeze-out (FO) [see Eqs. (9)–(26)], Cooper-Frye FO on a characteristic curve [Eq. (27)], and Milekhin FO on a characteristic curve [Eq. (27)]. These spectra were calculated within a 1D hydrodynamic expansion of the slab of initial width of 4 fm and initial energy density $\varepsilon_0 =$ 3 GeV/fm^3. Initial conditions for this slab are constructed on

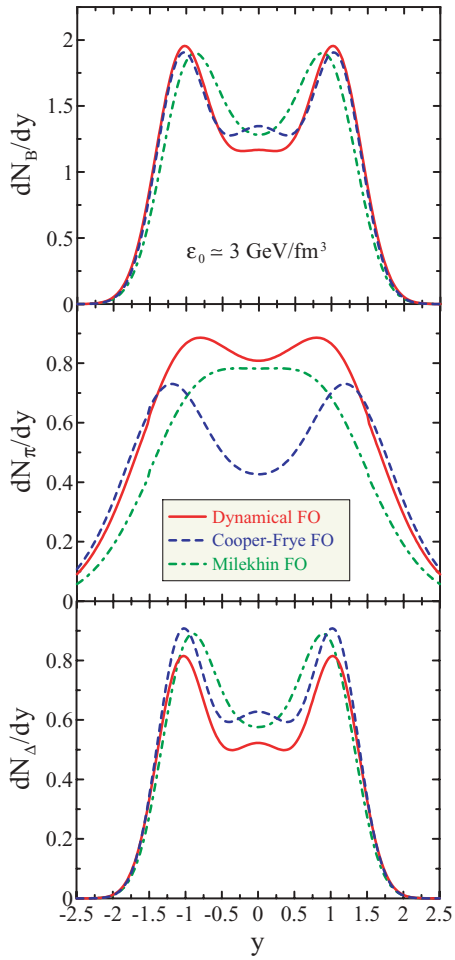

FIG. 5. (Color online) Rapidity distributions of baryons (upper panel), thermal pions (middle panel), and Δ isobars (lower panel) calculated within three models of freeze-out: the model of dynamical freeze-out (FO) [see Eqs. (9)–(26)], Cooper-Frye FO on the characteristic curve of Eq. (27), and Milekhin FO on the characteristic curve of Eq. (27).

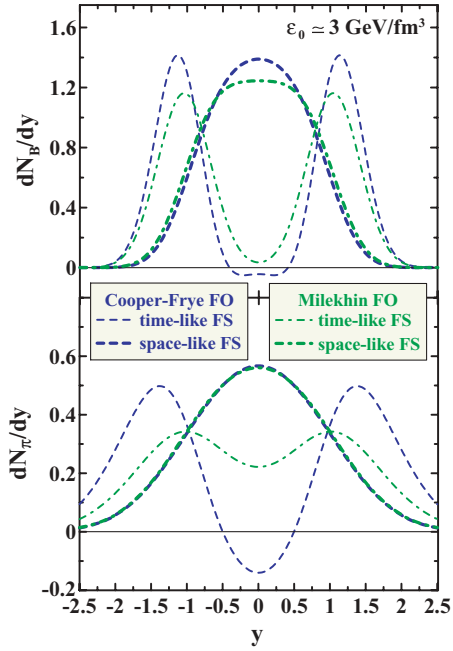

FIG. 6. (Color online) Partial contributions to rapidity spectra of baryons (upper panel) and thermal pions (lower panel) from spacelike and timelike parts of the freeze-out surface. Spectra are calculated within two models of freeze-out: Cooper-Frye FO on the characteristic curve of Eq. (27) and Milekhin FO on the same characteristic curve.

the assumption that it is formed by the shock-wave mechanism in a head-on collision of two 1D slabs at $E_{\rm lab} \simeq 10A$ GeV. Only nucleons, Δ's, and pions are included in the EOS used in this calculation. Displayed rapidity distributions are normalized to unit area transverse to the direction x of longitudinal expansion. Freeze-out surfaces for these three models of freeze-out are displayed in Fig. 1 for dynamical FO and in Fig. 4 (dashed curve for $\varepsilon = 0.4$ GeV/fm^3) for the Cooper-Frye FO and Milekhin FO.

It is difficult to directly compare the dynamical FO and Cooper-Frye FO, since the dynamical FO surface is inappropriate for the Cooper-Frye FO and vice versa. This is because the dynamical FO requires the hydrodynamics to be modified by removing the frozen-out matter, while the Cooper-Frye FO needs the hydrodynamic calculation to be run absolutely unrestricted. This is why we consider the Milekhin FO, which takes place precisely on the same characteristic curve [Eq. (27)] as the Cooper-Frye FO. In particular, this is why we compare only two models in Fig. 6.

As seen from Fig. 5, baryon rapidity distributions are quite close to each other within different freeze-out models. The dynamical FO and Cooper-Frye FO are even strikingly close. Apparently, this occurs because they are confined by the baryon number conservation. This is not the case for thermal pions (i.e., without contribution of Δ decays). The difference between their distributions within different models is quite spectacular.

As seen in Fig. 6, this difference mainly originates from contributions from the timelike[3] parts of the freeze-out surface, i.e., from those parts in which the the Cooper-Frye normal vector $n^\mu_{\rm CF}$ is spacelike: $n_{\rm CF} \cdot n_{\rm CF} < 0$. The difference between the Cooper-Frye and Milekhin recipes is most strongly pronounced in this case. Note that the Cooper-Frye FO even reveals its generic deficiency—its "timelike" spectrum becomes negative at midrapidity. Physically it means that the midrapidity region is most abundantly populated by particles which have to be returned to the hydrodynamic phase. At the same time, contributions from the spacelike parts of the surface, where $n_{\rm CF} \cdot n_{\rm CF} > 0$, are quite similar within the Cooper-Frye FO and Milekhin FO. The small difference between the Cooper-Frye normal timelike vector $n^\mu_{\rm CF}$ and the hydrodynamic four-velocity results is a tiny difference in timelike spectra.

Thus, spectra of newly produced particles are quite different in different models of freeze-out. At the same time, the

[3]We prefer to specify hypersurfaces by the character of space-time intervals within them, which is similar to Refs. [37,40] and contrary to Refs. [38,39].

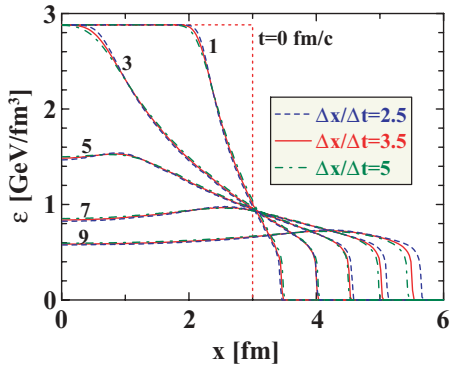

FIG. 7. (Color online) Same as Fig. 2 (top panel), but for different values of $\Delta x/\Delta t$. Only results with freeze-out are displayed.

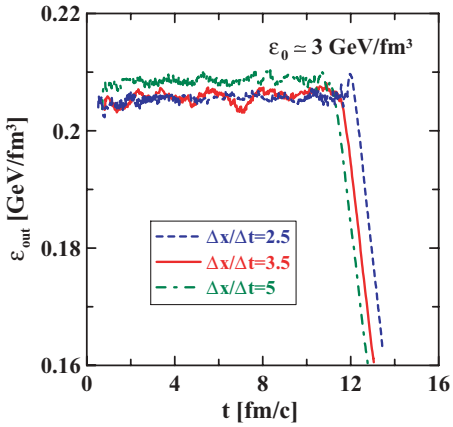

FIG. 8. (Color online) Same as Fig. 3, but for different values of $\Delta x/\Delta t$.

numerical baryon number and energy conservation is better than 1% in all considered models. We still face the question of which model is physically true. Unfortunately, the above-mentioned experiments on expansion of compressed and heated classical fluid into vacuum [48–51] cannot answer this question. As we have seen, particle number conservation (baryon number, in Fig. 5) makes these models fairly close to each other. We would like only to mention that the dynamical FO model naturally explains [14] the incident energy behavior of inverse-slope parameters of the transverse-mass spectra observed in experiments. However, this is not a physical justification of this model. The question still remains open.

Results of the above-reported 1D simulations are stable with respect to the numeric procedure [52]. They are quite insensitive to the size of the cell. The freeze-out front is smeared only over two cells independently of their size and hence indeed is steplike in the continuum limit. Dependence on the most important numeric parameter—the ratio of the space-grid step to the time step $\Delta x/\Delta t$—is displayed in Figs. 7 and 8. To reduce numerical diffusion, this ratio should be taken as optimal. As it was found in 1D simulations of exactly solvable problems [53], the optimal range of this ratio is $2.5 < \Delta x/\Delta t < 5$ with the preferable $\Delta x/\Delta t \simeq 3.5$, minimizing the numerical diffusion. As seen, within this range, $2.5 < \Delta x/\Delta t < 5$, the results are really stable.

D. 3D simulations

Condition (i) [or Eq. (18)] ensures only that the actual freeze-out energy density at which the freeze-out actually occurs is less than $\varepsilon_{\rm frz}$. Therefore, $\varepsilon_{\rm frz}$ can be called a "trigger" value of the freeze-out energy density. As demonstrated in the previous section, a natural value of this actual freeze-out energy density is $\varepsilon_{\rm out} \approx \varepsilon^s/2$, i.e., at the middle of the fall from ε^s to zero. To find out the actual value of $\varepsilon_{\rm out}$, we have to analyze results of a particular simulation. In our previous paper [6], we performed only a rough analysis of this kind. This is why in the main text of Ref. [6] we mentioned the value of approximately 0.2 GeV/fm^3 for $\varepsilon_{\rm out}$ and in the Appendix explained how the freeze-out actually proceeded.[4] Results of a more comprehensive analysis for central ($b = 0$) Pb+Pb collisions are presented in Fig. 9, which shows the $\varepsilon_{\rm out}$ value averaged over space-time evolution of the collision: $\langle\varepsilon_{\rm out}\rangle$. As seen, $\langle\varepsilon_{\rm out}\rangle$ reveals saturation at the SPS energies. This happens even though our freeze-out condition involves only a single constant parameter $\varepsilon_{\rm frz} = 0.4$ GeV/fm^3, with the exception of low incident energies, for which we use lower values: $\varepsilon_{\rm frz}(2A\ {\rm GeV}) = 0.3$ GeV/fm^3 and $\varepsilon_{\rm frz}(1A\ {\rm GeV}) = 0.2$ GeV/fm^3.

The steplike behavior of $\langle\varepsilon_{\rm out}\rangle$ is a consequence of the freeze-out dynamics, which has already been illustrated in Fig. 3. At low (AGS) incident energies, the energy density achieved at the border with vacuum, ε^s, is lower than $\varepsilon_{\rm frz}$. The surface freeze-out stays at this lower energy density up to the global freeze-out, because the freeze-out front cannot overcome the supersonic barrier in the expanding matter, cf. the lower panel of Fig. 2. At these low energies, the value $\langle\varepsilon_{\rm out}\rangle$ turns out to be of little sensitivity to the freeze-out parameter $\varepsilon_{\rm frz}$. Only the global freeze-out (iii b) of the system remnant, which also contributes to $\langle\varepsilon_{\rm out}\rangle$, produces weak

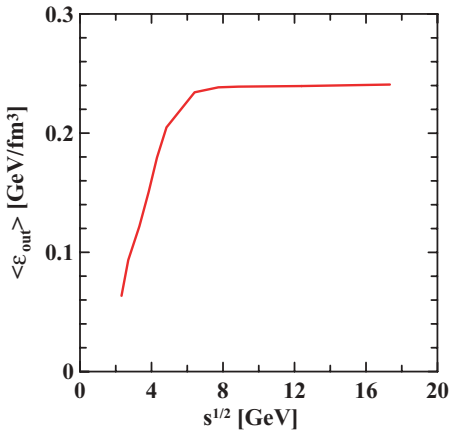

FIG. 9. (Color online) Actual average freeze-out energy density in central ($b = 0$) $Pb+Pb$ collisions as a function of invariant incident energy.

[4] In terms of Ref. [6] ($\varepsilon_{\rm frz[1]}$ and $\varepsilon^{\rm code}_{\rm frz[1]}$), our present quantities are $\varepsilon_{\rm frz} = \varepsilon^{\rm code}_{\rm frz[1]}$ and $\varepsilon_{\rm out} = \varepsilon_{\rm frz[1]}$.

sensitivity to $\varepsilon_{\rm frz}$. The values $\varepsilon_{\rm frz}(2A\ {\rm GeV}) = 0.3\ {\rm GeV/fm}^3$ and $\varepsilon_{\rm frz}\ (1A{\rm GeV}) = 0.2\ {\rm GeV/fm}^3$ were precisely chosen in order to reduce the contribution of the global freeze-out to $\langle\varepsilon_{\rm out}\rangle$.

With the incident energy rise, the energy density achieved at the border with vacuum gradually reaches the value of $\varepsilon_{\rm frz}$ and then even overshoots it. If the overshoot happens, the system first expands without freeze-out. The freeze-out starts only when ε^s drops to the value of $\varepsilon_{\rm frz}$. Then the surface freeze-out occurs really at the value $\varepsilon^s \approx \varepsilon_{\rm frz}$, and thus the actual freeze-out energy density saturates at the value $\langle\varepsilon_{\rm out}\rangle \approx \varepsilon_{\rm frz}/2$.

In Fig. 10, the time evolution of the total energy density [cf. Eq. (10)] in the central Pb+Pb collision at $E_{\rm lab} = 158A$ GeV is displayed. The light-colored outer halo corresponds to the simulation without freeze-out and thus indicates the matter which has already been frozen out to the time instant t. First of all, we see that already in the beginning of the expansion stage ($t = 2$ fm/c), the baryon-rich fluids are mutually stopped and unified to a good extent, since their hydrodynamic velocities almost coincide: arrows, originating from the same point, are almost equal if not merged. This is not the case for the baryon-free fluid, since its formation lasts until approximately $t = 4$ fm/c (see Fig. 18 in Ref. [6]). At the late stage of the expansion ($t \gtrsim 10$ fm/c), the baryon-rich and baryon-free fluids become even spatially separated: the middle region of the system, containing no arrows, is solely populated by the baryon-free fluid, and hence the baryon-rich matter falls into two disconnected pieces. Thus, at the late stage of the evolution, the system effectively consists of three fireballs (two baryon-rich and one baryon-free). This is in contrast to the assumption of the statistical model [55–58], where a single uniform fireball is considered. The baryon-free fireball becomes frozen out first: the displayed time instant $t = 11$ fm/c is almost the last, when this fireball still hydrodynamically evolves. Evolution of the two baryon-rich fireballs until the complete freeze-out is rather long, up to

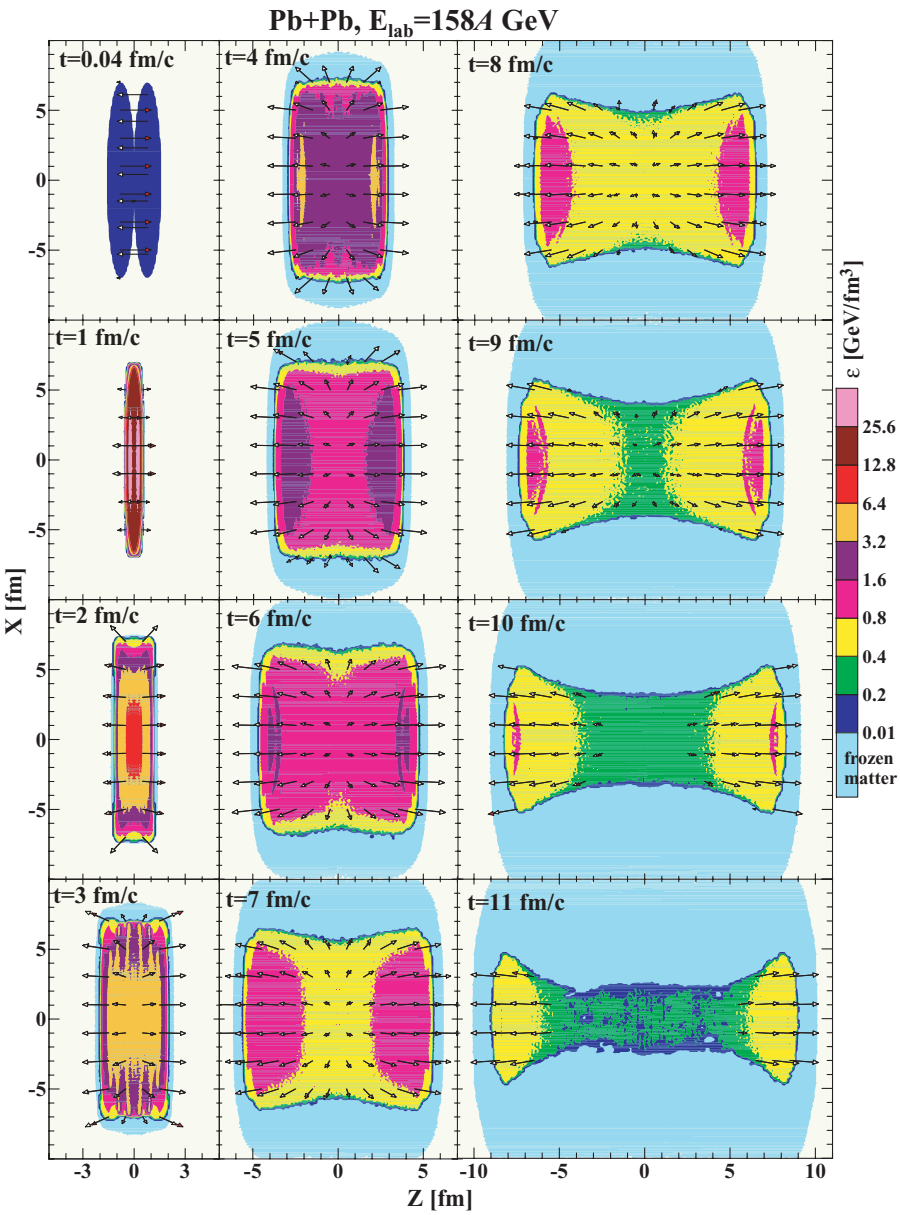

FIG. 10. (Color online) Time evolution (in the xz plane of the center-of-mass frame) of the total energy density [cf. Eq. (10)] in the central $Pb+Pb$ collision at $E_{\rm lab} = 158A$ GeV. The light-colored outer halo corresponds to the simulation without freeze-out and thus indicates the matter which has already been frozen out to the time instant t. Arrows indicate velocities of baryon-rich fluids: open arrows for the projectilelike fluid and filled arrows for the targetlike fluid.

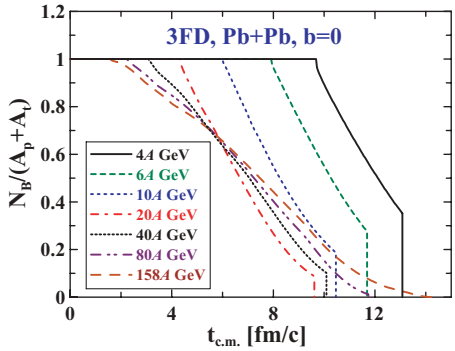

FIG. 11. (Color online) Time evolution (in the center-of-mass frame) of the non-frozen-out baryon number (normalized to the total baryon number of the system $A_p + A_t$) in central $Pb+Pb$ collisions at various incident energies.

$t \approx 20$ fm/c. This spatial separation of fireballs happens only at high incident energies $E_{\rm lab} > 40A$ GeV.

The freeze-out in the longitudinal direction proceeds according to the 1D pattern of Fig. 2 (upper panel). In the transverse direction, the freeze-out front moves into interior of the system. This a combined effect of the fast longitudinal expansion and the comparatively slow transverse motion of the system. This effect actually results in the two-fireball structure at the latest stage.

The occurrence of two spatially separated fireballs at the latest stage of the collision is the reason why the global freeze-out, cf. (iii b), does not occur in this system. At low (AGS) incident energies, the surface freeze-out, actually occurring at lower than $\varepsilon_{\rm frz}$ densities, takes place only as long as the energy density in the center of the expanding system exceeds $\varepsilon_{\rm frz}$. When this center density drops below $\varepsilon_{\rm frz}$, the rest of the system instantly gets frozen out, as illustrated in Fig. 11 at the example of time evolution of the baryon number still involved in the hydrodynamic phase. The abrupt fall of a curve corresponds to the global freeze-out. In fact, only this global freeze-out stage depends on the freeze-out parameter $\varepsilon_{\rm frz}$ at low incident energies. With the incident energy rise, this instantly frozen-out remnant becomes smaller and smaller until it completely disappears above $40A$ GeV energy. This happens because the outer freeze-out fronts stay already at the $\varepsilon_{\rm frz}$ density, therefore the maximum volume density can be only higher than $\varepsilon_{\rm frz}$. At the same time, the inner freeze-out fronts overtake these two baryon-rich fireballs from behind and result in gradual surface freeze-out of the fireballs without any remnant in which criterion (iii b) can work.

IV. CONCLUSIONS

The described method of freeze-out can be called dynamical, since the freeze-out process here is integrated into fluid dynamics through hydrodynamic equations (15)–(18). The freeze-out front is not defined just "geometrically" on the condition of the freeze-out criterion met but rather is a subject of the fluid evolution. It competes with the fluid flow and does not always reach the place where the freeze-out criterion is met.

This kind of freeze-out is similar to the model of continuous emission proposed in Ref. [46]. There, the particle emission occurs from a surface layer of the mean-free-path width. In our case, the physical pattern is similar, only the mean free path is shrunk to zero. In particular, the fact that the freeze-out sometimes occurs at lower energy densities than that prescribed by the freeze-out criterion can be associated with the dependence on the future evolution of the fluid system in the model of continuous emission. In that model, the particle emission occurs from the interior of the time-evolving system. Therefore, whether the emitted particle is able to leave the system or not depends on the expansion rate of the system. Similar situations happen in our model. Sometimes the freeze-out criterion is met too deeply inside the system such that rapid expansion of the system prevents the freeze-out front from reaching this place.

We argue that the Milekhin's original method [22] of calculating observable particle spectra is energy conserving, as well as the Cooper-Frye recipe [23], provided it is considered on a discontinuous hypersurface, i.e., that consisting of tiny (infinitely small in continuum limit) fragments with normal vectors coinciding with the local hydrodynamic four-velocity. Moreover, we argue that Milekhin's approach on a discontinuous hypersurface is natural for the Lagrangian formulation of hydrodynamics. There are no principal objections against using such a fragmented hypersurface instead of the continuous one as in the Cooper-Frye method. Discreetness of particle emission may hint at a discontinuous character of the freeze-out hypersurface.

Systematic studies based on hydrodynamic models indicate that there are two distinct freeze-out points (see, e.g., [59,60]): chemical and thermal ones. Contrary to these studies, we do not need two distinct freeze-out points. Multiplicities and spectra are simultaneously and quite satisfactorily reproduced with the single freeze-out described above [6]. Of course, we could somewhat refine reproduction of experimental data by introducing two distinct freeze-out points. However, introduction of an additional fitting parameter would be too high price for such a slight improvement.

ACKNOWLEDGMENTS

We are grateful to M. I. Gorenstein, E. E. Kolomeitsev, I. N. Mishustin, L. M. Satarov, V. V. Skokov, V. D. Toneev, and D. N. Voskresensky for fruitful discussions. This work was supported by Deutsche Forschungsgemeinschaft (DFG Project 436 RUS 113/558/0-3), Russian Foundation for Basic Research (RFBR Grant 06-02-04001 NNIO_a), and Russian Federal Agency for Science and Innovations (Grant NSh-8756.2006.2).

APPENDIX: PROBLEM OF FROZEN-OUT HADRONS RETURNING TO THE HYDRODYNAMIC PHASE

When frozen-out matter coexists with a still hydrodynamically evolving fluid, both the conventional Cooper-Frye

recipe [23] and the model presented here suffer from a problem of frozen-out particles returning to the hydrodynamic phase. For the Cooper-Frye method, this problem was discussed in a number of papers [37–40,42]. Here we would like to demonstrate that precisely the same (and precisely to the same extent) problem exists for the freeze-out model discussed in this paper.

Let the fluid and frozen-out matter be separated by a space surface with an external normal three-vector $\mathbf{n}$. Let this surface move with velocity $\mathbf{v}_\sigma$. Then we can decompose the number of particles frozen out on the element of hypersurface $d\sigma$, associated with the above separation surface, as follows [cf. Eq. (1)]

$$dN = dN_{\text{esc.}} + dN_{\text{ret.}}, \tag{A1}$$

$$dN_{\text{esc.}} = d\sigma n_\sigma^\mu \int \frac{d^3p}{p_0} p_\mu f(p,x)\,\Theta([\mathbf{v}-\mathbf{v}_\sigma]\cdot\mathbf{n}), \tag{A2}$$

$$dN_{\text{ret.}} = d\sigma n_\sigma^\mu \int \frac{d^3p}{p_0} p_\mu f(p,x)\,\Theta([\mathbf{v}_\sigma-\mathbf{v}]\cdot\mathbf{n}), \tag{A3}$$

where $\mathbf{v} = \mathbf{p}/p_0$ is the three-velocity of a frozen-out particle. Here $dN_{\text{esc.}}$ can be identified with a number of particles escaping from the system, since they move outward from the system faster than the free surface overtakes them. While $dN_{\text{ret.}}$ is a number of particles returning to the fluid. In the covariant form, Θ functions can be written as (see, e.g., Refs. [37–40])

$$\Theta([\mathbf{v}-\mathbf{v}_\sigma]\cdot\mathbf{n}) = \Theta\left(p_\mu n^\mu_{\text{CF}_\sigma}\right), \tag{A4}$$

$$\Theta([\mathbf{v}_\sigma-\mathbf{v}]\cdot\mathbf{n}) = \Theta\left(-p_\mu n^\mu_{\text{CF}_\sigma}\right), \tag{A5}$$

where $n^\mu_{\text{CF}_\sigma}$ is the normal four-vector to the Cooper-Frye continuous hypersurface. This is always so, independent of the choice of n^μ_σ we use for calculation of spectra. Therefore, the fraction of returning particles, $dN_{\text{ret.}}/dN_{\text{esc.}}$ is independent of whether we employ the Cooper-Frye recipe with $n^\mu_\sigma = n^\mu_{\text{CF}_\sigma}$ or Milekhin's method with $n^\mu_\sigma = u^\mu$.

[1] R. B. Clare and D. Strottman, Phys. Rep. **141**, 177 (1986).
[2] H. Stoecker and W. Greiner, Phys. Rep. **137**, 277 (1986).
[3] I. N. Mishustin, V. N. Russkikh, and L. M. Satarov, Yad. Fiz. **54**, 429 (1991) [Sov. J. Nucl. Phys. **54**, 260 (1991)].
[4] D. H. Rischke, arXiv:nucl-th/9809044v1.
[5] P. Huovinen and P. V. Ruuskanen, Ann. Rev. Nucl. Part. Sci. **56**, 163 (2006).
[6] Yu. B. Ivanov, V. N. Russkikh, and V. D. Toneev, Phys. Rev. C **73**, 044904 (2006).
[7] V. D. Toneev, Yu. B. Ivanov, E. G. Nikonov, W. Norenberg, and V. N. Russkikh, Phys. Part. Nucl. Lett. **2**, 288 (2005) [Pi'ma Fiz. Element. Chastits Atom. Yadra **2**, 43 (2005)]; V. N. Russkikh, Yu. B. Ivanov, E. G. Nikonov, W. Norenberg, and V. D. Toneev, Phys. At. Nucl. **67**, 199 (2004) [Yad. Fiz. **67**, 195 (2004)].
[8] I. N. Mishustin, V. N. Russkikh, and L. M. Satarov, Yad. Fiz. **48**, 711 (1988) [Sov. J. Nucl. Phys. **48**, 454 (1988)]; Nucl. Phys. **A494**, 595 (1989).
[9] Yu. B. Ivanov, E. G. Nikonov, W. Nörenberg, V. D. Toneev, and A. A. Shanenko, Heavy Ion Phys. **15**, 117 (2002).
[10] U. Katscher, D. H. Rischke, J. A. Maruhn, W. Greiner, I. N. Mishustin, and L. M. Satarov, Z. Phys. A **346**, 209 (1993); U. Katscher, J. A. Maruhn, W. Greiner, and I. N. Mishustin, Z. Phys. A **346**, 251 (1993); A. Dumitru, U. Katscher, J. A. Maruhn, H. Stöcker, W. Greiner, and D. H. Rischke, Phys. Rev. C **51**, 2166 (1995); Z. Phys. A **353**, 187 (1995).
[11] J. Brachmann, A. Dumitru, J. A. Maruhn, H. Stöcker, W. Greiner, and D. H. Rischke, Nucl. Phys. **A619**, 391 (1997); A. Dumitru, J. Brachmann, M. Bleicher, J. A. Maruhn, H. Stöcker, and W. Greiner, Heavy Ion Phys. **5**, 357 (1997); M. Reiter, A. Dumitru, J. Brachmann, J. A. Maruhn, H. Stöcker, and W. Greiner, Nucl. Phys. **A643**, 99 (1998); M. Bleicher, M. Reiter, A. Dumitru, J. Brachmann, C. Spieles, S. A. Bass, H. Stöcker, and W. Greiner, Phys. Rev. C **59**, R1844 (1999); J. Brachmann, A. Dumitru, H. Stöcker, and W. Greiner, Eur. Phys. J. A **8**, 549 (2000).
[12] J. Brachmann, S. Soff, A. Dumitru, H. Stöcker, J. A. Maruhn, W. Greiner, L. V. Bravina, and D. H. Rischke, Phys. Rev. C **61**, 024909 (2000).
[13] V. N. Russkikh and Yu. B. Ivanov, Phys. Rev. C **74**, 034904 (2006).
[14] Yu. B. Ivanov and V. N. Russkikh, arXiv:nucl-th/0607070v2.
[15] V. M. Galitsky and I. N. Mishustin, Sov. J. Nucl. Phys. **29**, 181 (1979).
[16] L. Ahle *et al.*, Phys. Lett. **B476**, 1 (2000).
[17] S. V. Afanasiev *et al.*, Phys. Rev. C **66**, 054902 (2002); V. Friese *et al.*, J. Phys. G **30**, S119 (2004); M. Gazdzicki *et al.*, J. Phys. G **30**, S701 (2004).
[18] M. I. Gorenstein, M. Gazdzicki, and K. Bugaev, Phys. Lett. **B567**, 175 (2003).
[19] B. Mohanty, Jan-e Alam, S. Sarkar, T. K. Nayak, and B. K. Nandi, Phys. Rev. C **68**, 021901(R) (2003).
[20] E. L. Bratkovskaya, M. Bleicher, M. Reiter, S. Soff, H. Stöcker, M. van Leeuwen, S. Bass, and W. Cassing, Phys. Rev. C **69**, 054907 (2004); E. L. Bratkovskaya, S. Soff, H. Stöcker, M. van Leeuwen, and W. Cassing, Phys. Rev. Lett. **92**, 032302 (2004).
[21] M. Gazdzicki, M. I. Gorenstein, F. Grassi, Y. Hama, T. Kodama, and O. Socolowski Jr., Braz. J. Phys. **34**, 322 (2004).
[22] G. A. Milekhin, Zh. Eksp. Teor. Fiz. **35**, 1185 (1958); Sov. Phys. JETP **35**, 829 (1959); Trudy FIAN **16**, 51 (1961).
[23] F. Cooper and G. Frye, Phys. Rev. D **10**, 186 (1974).
[24] D. H. Rischke, Y. Pürsün, J. A. Maruhn, H. Stöcker, and W. Greiner, Heavy Ion Phys. **1**, 309 (1995).
[25] J. Sollfrank, P. Huovinen, M. Kataja, P. V. Ruuskanen, M. Prakash, and R. Venugopalan, Phys. Rev. C **55**, 392 (1997); P. Huovinen, P. V. Ruuskanen, and J. Sollfrank, Nucl. Phys. **A650**, 227 (1999); P. F. Kolb, J. Sollfrank, P. V. Ruuskanen, and U. Heinz, Nucl. Phys. **A661**, 349 (1999); P. F. Kolb, J. Sollfrank, and U. Heinz, Phys. Lett. **B459**, 667 (1999); P. F. Kolb, P. Huovinen, U. Heinz, and H. Heiselberg, Phys. Lett. **B500**, 232 (2001).
[26] C. M. Hung and E. V. Shuryak, Phys. Rev. Lett. **75**, 4003 (1995); C. M. Hung and E. Shuryak, Phys. Rev. C **57**, 1891 (1998).
[27] D. Teaney, J. Lauret, and E. V. Shuryak, arXiv:nucl-th/0110037v2; Phys. Rev. Lett. **86**, 4783 (2001).
[28] T. Hirano, U. W. Heinz, D. Kharzeev, R. Lacey, and Y. Nara, arXiv:nucl-th/0701075.

[29] A. Dumitru, S. A. Bass, M. Bleicher, H. Stöcker, and W. Greiner, Phys. Lett. **B460**, 411 (1999); S. A. Bass, A. Dumitru, M. Bleicher, L. Bravina, E. Zabrodin, H. Stöcker, and W. Greiner, Phys. Rev. C **60**, 021902(R) (1999); S. A. Bass and A. Dumitru, *ibid*. **61**, 064909 (2000).
[30] D. Yu. Peressounko and Yu. E. Pokrovsky, Nucl. Phys. **A669**, 196 (2000).
[31] C. Nonaka, E. Honda, and S. Muroya, Eur. Phys. J. C **17**, 663 (2000).
[32] T. Hirano, Phys. Rev. C **65**, 011901(R) (2001); T. Hirano and K. Tsuda, *ibid*. **66**, 054905 (2002).
[33] Y. Hama, T. Kodama, and O. Socolowski, Braz. J. Phys. **35**, 24 (2005).
[34] C. Nonaka and S. A. Bass, Nucl. Phys. **A774**, 873 (2006); Phys. Rev. C **75**, 014902 (2007).
[35] T. Hirano, U. W. Heinz, D. Kharzeev, R. Lacey, and Y. Nara, Phys. Lett. **B636**, 299 (2006).
[36] L. M. Satarov, A. V. Merdeev, I. N. Mishustin, and H. Stocker, Phys. Rev. C **75**, 024903 (2007); L. M. Satarov, I. N. Mishustin, A. V. Merdeev, and H. Stöcker, arXiv:hep-ph/0611099v1.
[37] K. A. Bugaev, Nucl. Phys. **A606**, 559 (1996).
[38] J. J. Neumann, B. Lavrenchuk, and G. Fai, Heavy Ion Phys. **5**, 27 (1997).
[39] L. P. Csernai, Z. Lázár, and D. Molnár, Heavy Ion Phys. **5**, 467 (1997).
[40] K. A. Bugaev and M. I. Gorenstein, arXiv:nucl-th/9903072v2; K. A. Bugaev, M. I. Gorenstein, and W. Greiner, J. Phys. G **25**, 2147 (1999); Heavy Ion Phys. **10**, 333 (1999).
[41] Cs. Anderlik, L. P. Csernai, F. Grassi, Y. Hama, T. Kodama, Zs. Lázár, and H. Stöcker, Heavy Ion Phys. **9**, 193 (1999).
[42] K. Tamošiūnas and L. P. Csernai, Eur. Phys. J. A **20**, 269 (2004).
[43] Steven Weinberg, *Gravitation and Cosmology: Principles and Applications of the General Theory of Relativity* (Wiley, New York, 1972), Chap. 2, Secs. 6 and 8.
[44] M. I. Gorenstein and Yu. M. Sinyukov, Phys. Lett. **B142**, 425 (1984).
[45] E. Molnar, L. P. Csernai, V. K. Magas, A. Nyiri, and K. Tamošiūnas, Phys. Rev. C **74**, 024907 (2006).
[46] F. Grassi, Y. Hama, and T. Kodama, Phys. Lett. **B355**, 9 (1995); Z. Phys. C **73**, 153 (1996); Yu. M. Sinyukov, S. V. Akkelin, and Y. Hama, Phys. Rev. Lett. **89**, 052301 (2002); F. Grassi, Braz. J. Phys. **35**, 52 (2005).
[47] L. D. Landau and E. M. Lifshitz, *Fluid Mechanics* (Pergamon Press, Oxford, 1979).
[48] C. J. Knight, J. Fluid Mech. **75**, 469 (1976).
[49] J. E. Shepherd and B. Sturtevant, J. Fluid Mech. **121**, 379 (1982).
[50] Th. Kurschat, H. Chaves, and G. E. A. Meier, J. Fluid Mech. **236**, 43 (1992).
[51] J. R. Simoes-Moreira and J. E. Shepherd, J. Fluid Mech. **382**, 63 (1999).
[52] A. S. Roshal and V. N. Russkikh, Yad. Fiz. **33**, 1520 (1981).
[53] V. N. Russkikh, in *Numerical Methods of Medium Mechanics* (in Russian) (Novosibirsk, 1987) Vol. 1(18), p. 104.
[54] F. H. Harlow, A. A. Amsden, and J. R. Nix, J. Comput. Phys. **20**, 119 (1976).
[55] A. Andronic, P. Braun-Munzinger, and J. Stachel, Nucl. Phys. **A772**, 167 (2006).
[56] J. Cleymans, H. Oeschler, K. Redlich, and S. Wheaton, Phys. Rev. C **73**, 034905 (2006); J. Phys. G **32**, S165 (2006).
[57] J. Randrup and J. Cleymans, Phys. Rev. C **74**, 047901 (2006).
[58] A. Dumitru, L. Portugal, and D. Zschiesche, Phys. Rev. C **73**, 024902 (2006).
[59] E. V. Shuryak, Nucl. Phys. **A661**, 119c (1999).
[60] U. Heinz, Nucl. Phys. **A661**, 141c (1999).